Industrial Crops & Products 235 (2025) 121715

Contents lists available at ScienceDirect

Industrial Crops & Products

journal homepage: www.elsevier.com/locate/indcrop

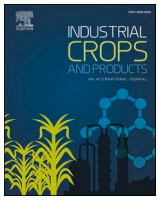

Light-induced Dof transcription factors up-regulate the andrographolide biosynthesis in *Andrographis paniculata*

Xingbin Lv [a,b,1], Hua Yang [a,1], Yufang Hu [a], Tingting Jing [a,d], Ying Xiong [a], Qi Liang [a,c], Shuyun Tian [a], Lang Yang [a], Zhiyi Zhang [a,c], Mingkun Huang [a,c], Yanqin Xu [b], Ling Zhang [a,c,*]

[a] *Jiangxi Provincial Key Laboratory of Ex Situ Plant Conservation and Utilization, Lushan Botanical Garden, Chinese Academy of Sciences, 9 Zhiqing Road, Jiujiang, Jiangxi 332900, China*
[b] *School of Pharmacy, Jiangxi University of Traditional Chinese Medicine, 1688 Meiling Avenue, Xinjian Dis-trict, Nanchang, Jiangxi 330004, China*
[c] *Nanchang University, 999 Xuefu Avenue, Honggutan New District, Nanchang, Jiangxi 330047, China*
[d] *Guangdong Provincial Key Laboratory of Applied Botany & State Key Laboratory of Plant Diversity and Specialty Crops, South China Botanical Garden, Chinese Academy of Sciences, Guangzhou 510650, China*

ARTICLE INFO

Keywords:
Andrographis paniculata
Dof transcription factor
Light
Andrographolide

ABSTRACT

Andrographis paniculata (*A. paniculata*) is a traditional Chinese medicinal plant that accumulates andrographolide, a key bioactive diterpenoid compound. In this study, we found that light can upregulate the production of andrographolide. However, the underlying regulatory mechanisms governing its biosynthesis remain elusive. By coupling the RNA-seq data obtained under different light conditions with co-expression analysis, two candidate transcription factors, *ApDof16* and *ApDof29*, were identified. Using virus-induced gene silencing (VIGS), we demonstrated that these two Dofs were able to regulate the content of andrographolide as well as the expression of *ApCPS2*, a key gene of the andrographolide biosynthesis pathway. Further experiments, such as the yeast one-hybrid (Y1H) assays, transient assays and chromatin immunoprecipitation quantitative PCR (ChIP-qPCR) analysis indicated that *ApDof29* rather than *ApDof16*, directly binds to the promoter of *ApCPS2*, thereby regulating its expression and the subsequent andrographolide accumulation in response to light.

1. Introduction

Andrographis paniculata (L.) Heynh (*A. paniculata*) belongs to the family Acanthaceae (Okhuarobo et al., 2014). It is primarily distributed in regions such as India, Sri Lanka, and China (Gonde et al., 2024). Because of its bitter taste, it is also known as the "king of bitters" (Intharuksa et al., 2022). The plant exhibits various pharmacological activities including anti-inflammatory (Li et al., 2022), antioxidant (K et al., 2006), immunomodulatory (Chalichem et al., 2024), anticancer (Paul et al., 2021), and anti-HIV (Uttekar et al., 2012) effects. Its medicinal properties are primarily attributed to its diterpenoid compounds, such as andrographolide and neoandrographolide (Vetvicka and Vannucci, 2021a). Just as with other well-known medicinal plants, such as *Anemarrhena asphodeloides Bge.*, *Rhizoma Coptidis* and *Evodia rutaecarpa*, the therapeutic value of *Andrographis paniculata* is determined by its unique active ingredients (Cao et al., 2024; Gao et al., 2025a, 2025b). However, increasing clinical demand for andrographolide is severely limited by its low natural occurrence in the plant and degradation of germplasm resources (Chen et al., 2023b; Smitha et al., 2020). This supply–demand conflict highlights the urgent need to develop strategies to enhance the yield and quality of andrographolide by gaining a deep understanding of its biosynthetic pathway and transcriptional regulation.

As a secondary metabolite, the content of andrographolide is easily influenced by environmental factors such as light (Jones, 2018; Srinath et al., 2022a), which cause fluctuations in its accumulation and impact the quality of medicinal extracts. Light is not only essential for plant growth, development, and metabolism (Kusnetsov et al., 2020), but also influences many important physiological processes, such as seed germination (Jiang et al., 2016), de-etiolation (Armarego-Marriott et al.,

* Corresponding author at: Jiangxi Provincial Key Laboratory of Ex Situ Plant Conservation and Utilization, Lushan Botanical Garden, Chinese Academy of Sciences, 9 Zhiqing Road, Jiujiang, Jiangxi 332900, China.
E-mail address: linzh00@126.com (L. Zhang).
[1] Co-first authors

https://doi.org/10.1016/j.indcrop.2025.121715
Received 27 May 2025; Received in revised form 5 August 2025; Accepted 8 August 2025
Available online 12 August 2025

2020), root or shoot development (Lee et al., 2017), secondary metabolite synthesis (Zhang et al., 2021b), etc. However, the manner in which light regulates the content of andrographolide remains unclear. This knowledge gap poses a significant obstacle to optimising cultivation, particularly in the context of smart greenhouses, which provide unparalleled opportunities for precise environmental control to ensure high-quality plant production (Pereira et al., 2021).

Through transcriptome sequencing, co-expression analysis, and molecular biology experiments, in this study, we identified two Dof transcription factors (*ApDof16* and *ApDof29*) that regulate andrographolide biosynthesis in *A.paniculata*. These factors bind to the promoter of *ApCPS2*, a key gene in the andrographolide biosynthetic pathway, in response to light. Our findings reveal a new molecular mechanism by which light quality modulates andrographolide biosynthesis, providing critical insights into the regulatory network of plant secondary metabolism as well as forming a theoretical foundation for genetic improvement and germplasm innovation of *A. paniculata* in the future.

2. Methods

2.1. Experimental Materials

Seeds of *A. paniculata* were sown in round pots with a diameter of 12 cm containing peat soil-vermiculite mixture at a ratio of 1:1 (v/v). These pots were placed in a growth incubator set at 25 °C. After sowing, pots were covered with aluminium foil to exclude light for three days to facilitate germination. The germinated seeds were then divided into five treatment groups: Dark (D), White Light (L), Red Light (R), Blue Light (B), and Far-red Light (F). Group D was grown under continuous darkness for seven days, while groups L, R, B, and F were exposed to white, red, blue, or far-red light, respectively for 24 h a day at a photosynthetic photon flux density (PPFD) of 150 μmol·m^{-2}·s^{-1} (equivalent to ~15,000 lux) for an additional seven days.

For each treatment, tissues from light-treated seedlings were harvested from three biological replicates (n = 3). From each replicate, 5 g of tissue was rapidly frozen in liquid nitrogen and stored at −80 °C for andrographolide content analysis via HPLC. Additionally, 100 mg of tissue from each replicate was frozen in the same way for subsequent RNA extraction and gene expression analysis.

2.2. Measurement of Andrographolide Content

Andrographolide standard (Shanghai Yuanye Biotechnology Co., Ltd., China) was dissolved in methanol and sonicated for 10 min to ensure complete dissolution, then it was diluted to a final concentration of 1 mg/mL in a volumetric flask. For sample preparation, frozen tissues (-80 °C) were ground into a fine powder under liquid nitrogen. An aliquot of 0.04 g of each powdered sample was accurately weighed using an analytical balance and transferred to a 2 mL centrifuge tube. The sample in the tube was extracted with 1.8 mL of methanol (MERK, USA). The mixture was sonicated for 20 min to enhance extraction efficiency and centrifuged at 5000 × *g* for 8 min. The supernatant was collected, and both the standard solution and sample extracts were filtered through a 0.45 μm nylon membrane before HPLC analysis.

The HPLC analysis was conducted according to a previously established method (Chen et al., 2020), using a Waters e2695 system and a Zorbax SB-C18 column (4.6 × 150 mm, 5 μm) at 25 °C. The detection wavelength was set at 205 nm, and the mobile phase consisted of acetonitrile (A) and water (B) with the following gradient elution programme: 0–8 min, 21 %–25 % A; 8–20 min, 25 %–28 % A; 20–25 min, 28 %–85 % A; 25–30 min, 85 % A. The flow rate was maintained at 1.0 mL/min, and the injection volume was 10 μL. Calibration curves were generated using the standard solution to quantify the content of andrographolide in the samples based on peak area integration.

2.3. RNA Extraction and Library Construction

Total RNA was extracted from *A. paniculata* seedlings that had been subjected to different light treatments using the RNeasy Plant Mini Kit (QIAGEN, Germany), following the manufacturer's instructions. To remove genomic DNA contamination, the extracted RNA was treated with RNase-free DNase I (NEB, USA) for 30 min at 37 °C and subsequently purified using the RNA Clean & Concentrator Kit (Zymo, USA) to enhance RNA integrity and yield.

The mRNA was isolated from total RNA using Dynabeads™ Oligo (dT)$_{25}$ magnetic beads (Invitrogen, USA) according to the manufacturer's instructions. Transcriptome library construction was performed as described previously (Huang et al., 2024), involving reverse transcription of mRNA into first-strand cDNA, second-strand synthesis, end repair, dA-tailing, adapter ligation, and PCR-based library amplification. Libraries were purified using Agencourt AMPure XP beads (Beckman Coulter, USA) to remove short fragments and contaminants. Paired-end sequencing (150 bp, PE150) was conducted on an Illumina NovaSeq 6000 platform to generate high-throughput sequencing data for subsequent transcriptomic analysis.

2.4. RNA-seq Analysis

Raw RNA-seq data were processed for quality control using TrimGalore v0.6.10 (https://github.com/FelixKrueger/TrimGalore), a wrapper tool that integrates Cutadapt and FastQC, to remove sequencing adapters, low-quality bases (Phred score ≤ 20), and short reads (< 30 bp). Quality-filtered paired-end reads were aligned to the *A. paniculata* reference genome (10.6084/m9.figshare.24986769) using HISAT2 v2.2.1 (Kim et al., 2019) with default alignment parameters. Gene expression levels were quantified using Cuffnorm v2.2.1 (http://cole-trapnell-lab.github.io/cufflinks/cuffnorm), which normalises library sizes and calculates fragments per kilobase of transcript per million mapped reads (FPKM) values. The analysis utilized the reference transcriptome annotation (in GTF format) and input BAM files from aligned reads, applying the default library normalization method (classic-fpkm) and assuming unstranded library type (fr-unstranded). Differential expression analysis was performed using Cuffdiff v2.2.1 to identify genes with significant expression changes based on the following criteria: *p*-value ≤ 0.05, false discovery rate (FDR, *q*-value) ≤ 0.05, and absolute fold change ≥ 1.5. The genes met these thresholds were defined as differentially expressed genes (DEGs) for subsequent functional enrichment analysis.

2.5. GO Enrichment Analysis and Transcription Factor Annotation

To identify the major biological functions of the DEGs, we performed Gene Ontology (GO) enrichment analysis by TBtools software (Chen et al., 2023a), with setting *p*-value of ≤ 0.05 set as the significance threshold. Transcription factors were annotated from the *A. paniculata* protein sequences using the iTAK software (Zheng et al., 2016).

2.6. Co-expression Analysis

Pearson correlation analysis was conducted between differentially expressed TFs and DEGs involved in andrographolide biosynthesis, with gene pairs defined as co-expressed if they met |Pearson correlation coefficient (PCC)| ≥ 0.7 and *p*-value ≤ 0.05. To identify potential regulatory motifs, the FIMO v5.5.7 algorithm (Grant et al., 2011) was used to scan the promoter regions (2 kb upstream of the transcription start site (TSS)) of biosynthesis-related genes for overrepresented TF-binding sites, with a significance threshold of *p*-value < 10^{-4} in order to identify potential regulatory motifs. Transcription factor motif profiles were obtained as Position Weight Matrices (PWMs) from the PLANTPAN 4.0 database (Cn et al., 2019). The resulting potential regulatory network was visualised using Cytoscape v3.10.3 (https://github.com/cytoscape/

cytoscape), where nodes represent TFs or biosynthesis genes, and edges denote significant co-expression (PCC criteria) or predicted TF-DNA binding (FIMO motifs).

2.7. Gene Family Analysis of the DNA-binding with one finger (Dof)

Based on the iTAK annotation, Dof family genes were selected. Their exon-intron structures were visualised using TBtools. Then, we used MEGA (Tamura et al., 2021) to align multiple sequences and construct a phylogenetic tree using the Neighbor-Joining method with default parameters and 1000 bootstrap replicates. The constructed phylogenetic tree was visualized by iTOL (http://itol.embl.de/). The conserved motifs of the Dof family were identified using MEME (http://meme-suite.org/tools/meme) with default parameters.

2.8. Virus-induced Gene Silencing (VIGS) assay

The *ApDof16* and *ApDof29* fragments were individually cloned into the pLY156 (pTRV2) vector between the *Bam*HI and *Xho*I sites. Vector construction procedures are followed the method mentioned above, and the primers are listed in Table S1. Subsequently, the constructed plasmids, including pTRV1, pTRV2-Dofs, and the pTRV2 empty vector, were separately transformed into competent *Agrobacterium tumefaciens* GV3101 (pSoup) cells and selected by 50 μg·mL^{-1} kanamycin and 50 μg·mL^{-1} rifampicin. The cultures were then incubated overnight at 28℃ with shaking at 200 rpm and grown until the OD_{600} reached approximately 1.0. The bacterial cells were harvested by centrifugation and resuspended in infiltration buffer (10 mM $MgCl_2$, 10 mM MES, pH 5.6, 100 mM acetosyringone) and adjusted to an OD_{600} of 0.2. Equal volumes of pTRV1 and pTRV2 (either the empty vector or containing the insert fragments were mixed at a 1:1 ratio. Healthy *A. paniculata* at the four-leaf stage were selected and then infiltrated with the culture mixture using the vacuum infiltration method. After vacuum treatment, the plants were rinsed with water and cultured under normal greenhouse conditions for 10 days for use in andrographolide content analysis (described above) and quantitative real-time PCR (qPCR) analysis.

For the qPCR assay, total RNA was extracted using the Polysaccharide-Polyphenol Plant Total RNA Extraction Kit (Vazyme, China). The cDNA was synthesized by reverse transcription using the HiScript III RT SuperMix for qPCR (+gDNA wiper) kit (Vazyme, China) according to the manufacturer's instructions. Then, qPCR was performed to determine the relative expression levels of *ApDof16*, *ApDof29*, and *ApCPS2* using the cDNA as a template. *ApACT* served as the internal gene for normalization, and the primer sequences are listed in Table S1. The 20 μL qPCR reaction mixture contained: 10 μL of 2 × ChamQ Universal SYBR qPCR Master Mix, 0.4 μL each of forward and reverse primers, 1 μL of cDNA, and 8.2 μL of ddH_2O. The thermocycling programme was initial denaturation at 95 ℃ for 30 s; 40 cycles of 95 ℃ for 10 s and 60 ℃ for 30 s; followed by a melting curve analysis (95 ℃ for 15 s, 60 ℃ for 60 s, 95 ℃ for 15 s).

2.9. Subcellular Localization of ApDof16 and ApDof29

The CDS of *ApDof16* and *ApDof29* were amplified using the high-fidelity enzyme KOD (TOYOBO, Japan) and cloned into the pGreen-35S-GFP vector using *Hin*dIII and *Bam*HI to generate 35S:*ApDof16*-GFP and 35S:*ApDof29*-GFP vectors. The resulting vectors transformed into the *Agrobacterium tumefaciens* GV3101 (pSoup) and were infiltrated into *Nicotiana benthamiana* leaves. GFP fluorescence signals were then observed under a confocal microscope. The primers are listed in Table S1.

2.10. Yeast One-Hybrid Assay for ApDof16 and ApDof29

The bait vector pAbAi-*pApCPS2* was generated by inserting the previously obtained *pApCPS2* DNA sequence into the pAbAi vector via homologous recombination. Meanwhile, *ApDof16* and *ApDof29* were cloned into the yeast expression vector pGADT7, yielding the effector vectors pGADT7-*ApDof16* and pGADT7-*ApDof29*. The primer sequences are presented in Table S1. The bait plasmid was linearised with the restriction enzyme *Bst*BI and then transformed into competent Y1H Gold yeast cells to create the bait yeast strain. Positive yeast transformants, verified by PCR, were subsequently inoculated onto SD/ - Ura solid medium supplemented with varying concentrations of Aureobasidin A (AbA). The cultures were incubated at 30 °C for 3–5 days to establish the minimum AbA concentration that inhibited the growth of pAbAi - *pApCPS2* yeast cells. The constructed pGADT7-Dofs plasmids were introduced into these competent cells using the PEG/LiAC method, resulting in the generation of effector yeast strains. Positive yeast transformants were selected by plating on SD/-Leu solid medium and incubating at 30 °C for 3–4 days. For the interaction assay, serially diluted transformed cells were prepared and inoculated onto SD/ - Leu plates without AbA (Control) and plates containing 300 mM AbA. The plates were then incubated at 30 °C for 3–5 days.

2.11. Dual-luciferase Reporter Assay for Transcriptional Activity of ApDof16 and ApDof29

The *ApCPS2* promoter (*pApCPS2*) was amplified from leaf DNA using the high-fidelity enzyme KOD (TOYOBO, Japan). The CDS of *ApDof16* and *ApDof29* was subsequently amplified from leaf cDNA. The 50 μL PCR reaction mixture contained: 5 μL of 10 × PCR buffer, 5 μL of 2 mM dNTPs, 3 μL of 25 mM $MgSO_4$, 1.5 μL of each primer (forward and reverse), 1 μL of DNA, and 33 μL of ddH_2O. The amplification program consisted of initial denaturation at 94 ℃ for 2 min; 35 cycles of 98 ℃ for 10 s, 58 ℃ for 30 s, and 68 ℃ for 1 min; followed by a final extension at 68 ℃ for 10 min. Using homologous recombination, the amplified *pApCPS2* fragment was cloned into the linearized pGreenII 0800-LUC vector to generate pApCPS2:LUC vector, while the *ApDof16* and *ApDof29* pGreenII 62-SK vector between *Bam*HI and *Kpn*I site using Seamless cloning master mix to generate 35S: Dof vectors for overexpression vector assay. All the primers are listed in Table S1.

The constructed vectors, including *pApCPS2*:LUC, *ApDof16*-pGreenII 62-SK, and *ApDof29*-pGreenII 62-SK, were separately transformed into the competent *Agrobacterium tumefaciens* strain GV3101 (pSoup). Positive colonies identified by antibiotic selection and colony PCR were subsequently inoculated into liquid LB medium with 50 μg·mL^{-1} kanamycin and 50 μg·mL^{-1} rifampicin, and cultured overnight at 28℃ with shaking at 200 rpm. *Agrobacterium* cultures were grown to an OD_{600} of 0.5–1.0. The bacterial cells were then harvested by centrifugation at 4000 g for 5 min. The cell pellet was washed twice with infiltration buffer (10 mM $MgCl_2$, 10 mM MES, pH 5.6). The cells were resuspended in infiltration buffer containing 100 mM acetosyringone. Then, two *Agrobacterium* suspensions designated for infiltration were mixed at a 1:1 vol ratio, adjusting the OD_{600} of each suspension to 0.1–0.5. Fully expanded leaves from approximately one-month-old tobacco plants were selected. The prepared mixed *Agrobacterium* suspension was then infiltrated into the tobacco leaves using a 1 mL needleless syringe. For each vector combination, 5–10 leaves were infiltrated. Following infiltration, the plants were incubated overnight in darkness under normal greenhouse conditions and then transferred to normal light conditions for 24–48 h. The transformed leaf was sprayed with a reaction buffer containing 1 mM luciferin substrate and the luminescence signal was observed via a plant in *vivo* imaging system (Tanon 5200, China).

2.12. ChIP-qPCR Analysis of ApDof16 and ApDof29

Agrobacterium strain GV3101 (pSoup) harboring 35S:*ApDof16*-GFP and 35S:*ApDof29*-GFP was infiltrated into the abaxial epidermis of *A. paniculata* leaves. Following infiltration, the leaves were incubated in darkness for 1 day and subsequently transferred to normal light

conditions for 3 days. The infiltrated leaves were fixed with 1 % formaldehyde. Chromatin Immunoprecipitation (ChIP) was then performed following the protocol described previously (Zhang et al., 2023). Primers used for qPCR analysis are listed in Table S1. The region amplified by primer P1 served as a negative control. Relative enrichment was calculated by comparing the abundance of the target fragment in ChIP samples to that in Input samples. Values were then normalized relative to the signal obtained from the P1 region.

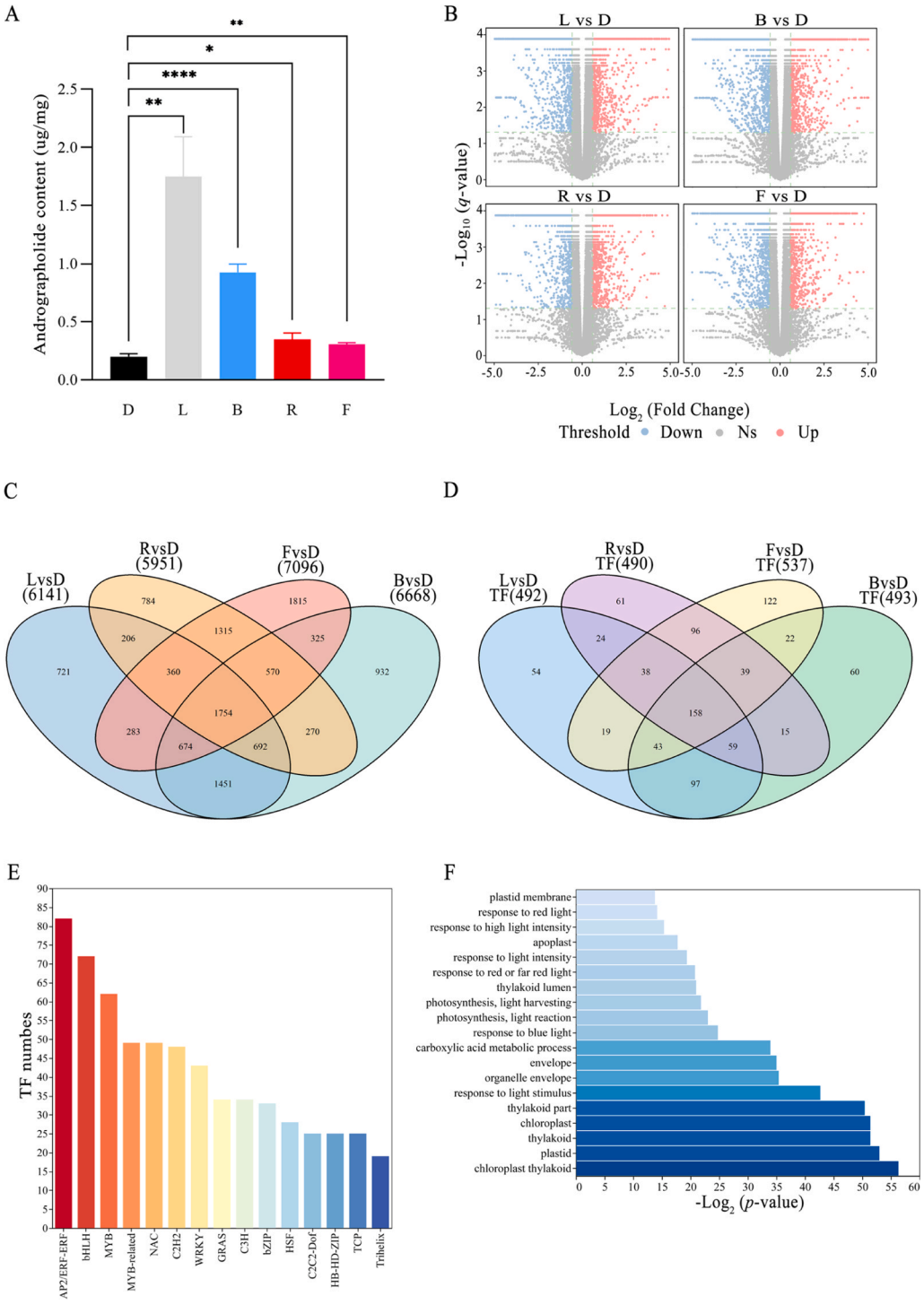

Fig. 1. The effect of light on the content of andrographolide and intrinsic gene expression in *A. paniculata* seedlings. (A) The andrographolide content of *A. paniculata* grown under various light conditions. The data are presented as the mean ± standard deviation (n = 3). Statistical significance is denoted by asterisks (*P < 0.05, **P < 0.01, ****P < 0.001 by Student's *t*-test). (B) Volcano plots display the differentially expressed genes (DEGs) in A. paniculata seedlings grown in light (L, B, R, F) or in darkness (D). DEGs were identified with a Log2 fold change ≥ 0.58 and a p-value ≤ 0.05. L, B, R, F, D indicate white light, blue light, red light, far-red light and dark-grown *A. paniculata* seedlings, respectively. (C) Venn diagrams were used for comparative analysis of DEGs. (D) Venn diagrams were used to conduct a comparative analysis of differentially expressed transcription factors. (E) The number of transcription factors in each family. (F) Gene ontology (GO) enrichment analysis of the DEGs.

3. Result

3.1. Light Upregulates the Andrographolide Biosynthesis

As Fig. 1A showed, the lowest andrographolide content accumulation (0.20 μg/mg) was observed in the seedlings that were grown in the complete dark (D) condition. In contrast, those seedlings grown in different light conditions, such as white light (L), Blue light (B), Red light (R) and Far-red light (F), significantly accumulate higher andrographolide content. Among them, the L and B group showed relatively high content (up to 1.75 and 0.93 μg/mg), while the R and F groups showed content of around 0.35 and 0.31 μg/mg, respectively.

To further understand the molecular mechanism of light regulating the andrographolide, we performed the RNA-seq using the seedlings from different light treatment (D, L, B, R, F), generating a total of 267.1 M RNA-seq raw reads (Table S1, Figure S1). Differential gene expression analysis was then conducted by comparing the light-grown groups to those grown in the dark. In total of 6141, 6668, 5951, 7096 DEGs were found in L versus D (L vs D) groups, B vs D, R vs D and F vs D (Figs. 1B and 1C), respectively. Among these DEGs, a total of 907 transcription factors have been identified (Figs. 1D and 1E). Gene Ontology (GO) enrichment analysis based on the DEGs showed several terms related to light or secondary metabolism were significantly enriched, such as Response to Light Stimulus (GO:0009416 and GO:0019684), Response to Red Light (GO:0010114), Response to Light Intensity (GO:0009642), Response to Blue Light (GO:0009637), and Response to Red or Far-red Light (GO:0009639) (Fig. 1F).

Furthermore, as previously reported (Sun et al., 2019a), andrographolide biosynthesis relies on two pathways, the mevalonate (MVA) pathway,the methylerythritol phosphate (MEP) pathway and Major

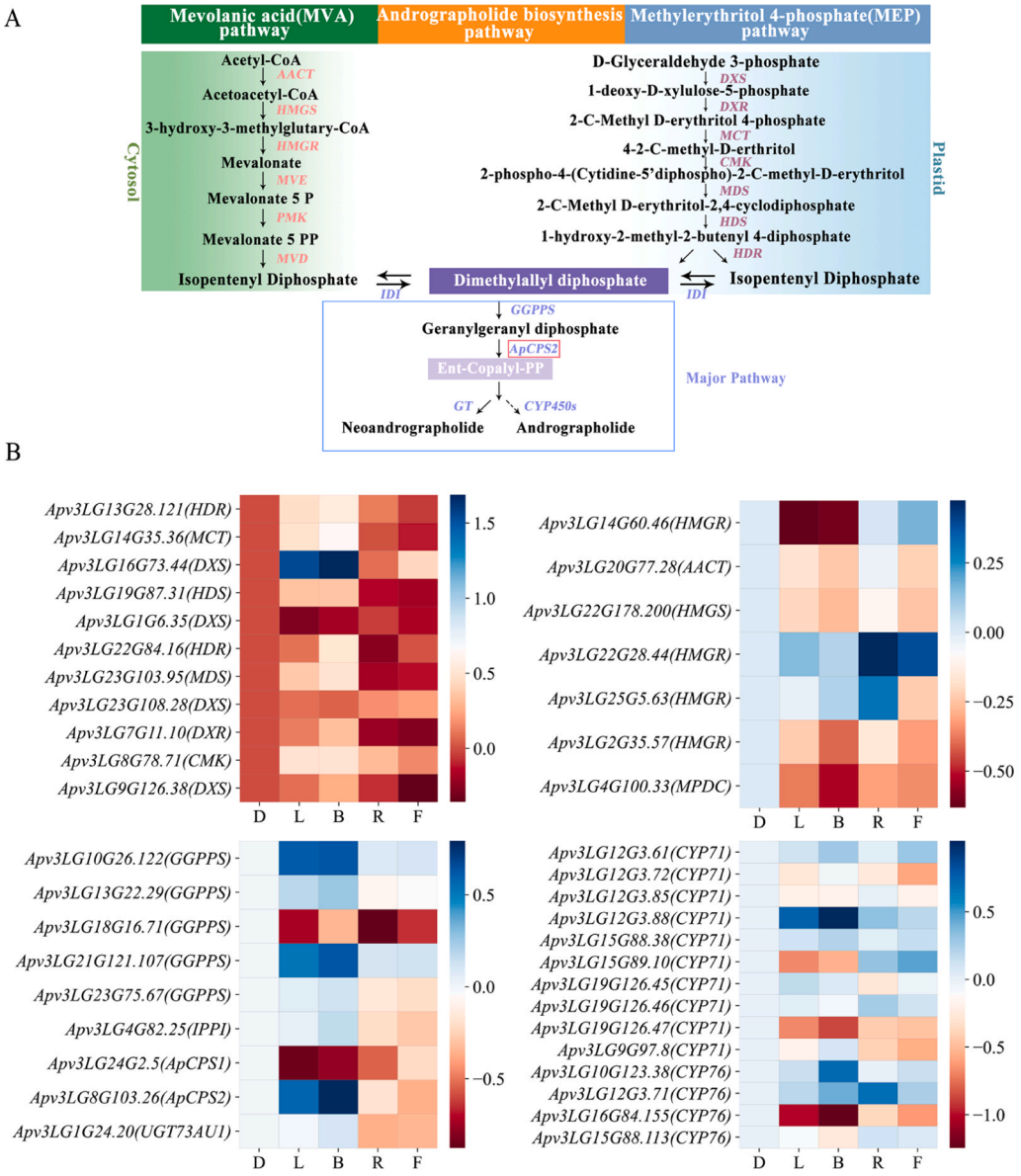

Fig. 2. Expression of andrographolide biosynthesis related genes (ABRGs) in light treatments. (A) A schematic representation of the andrographolide biosynthetic pathway and its associated genes in *A. paniculata.* The key gene, *ApCPS2,* is shown by a red square. Genes marked in red are from the MVA pathway, those in purple are from the MEP pathway, and genes in blue are involved in the downstream andrographolide biosynthesis, as demonstrated in the blue box at the bottom, which represents the major pathway leading to andrographolide and neoandrographolide formation. (B) Heatmaps show the relative expression levels of ABRGs under different light conditions. L, B, R, F and D indicated the white light, blue light, red light and far-red light and dark grown *A. paniculata* seedlings. The color scale of the heatmaps represents the $\log_{10}$ fold changes, which are normalized to the Fragments Per Kilobase of exon model per Million mapped fragments (FPKM) values of the seedlings grown under dark conditions (D).

pathway (Fig. 2A). In total, 69 andrographolide biosynthesis-related genes (ABRGs) have been identified in the genome, including the genes from the MEP pathway (e.g., *HDR*, *MCT*, *DXS*, *HDS*, *CMK*, *DXR*), the MVA pathway (e.g., *AACT*, *HMGS*, *HMGR*, *MPDC*), and other key enzyme genes such as *GGPPS*, *IPPI*, *CPS1*, *CPS2* (*ApCPS2*), *UGT73 AU1*, and *CYPs*. Based on the RNA-seq results, 41 ABRGs (59.4 %), such as the *HDR*, *MCT*, *DXS*, *HMGR*, *AACT*, *GGPPS*, *ApCPS2* etc., exhibited significant changes in light (L, B, R, F) compared to dark (D) grown

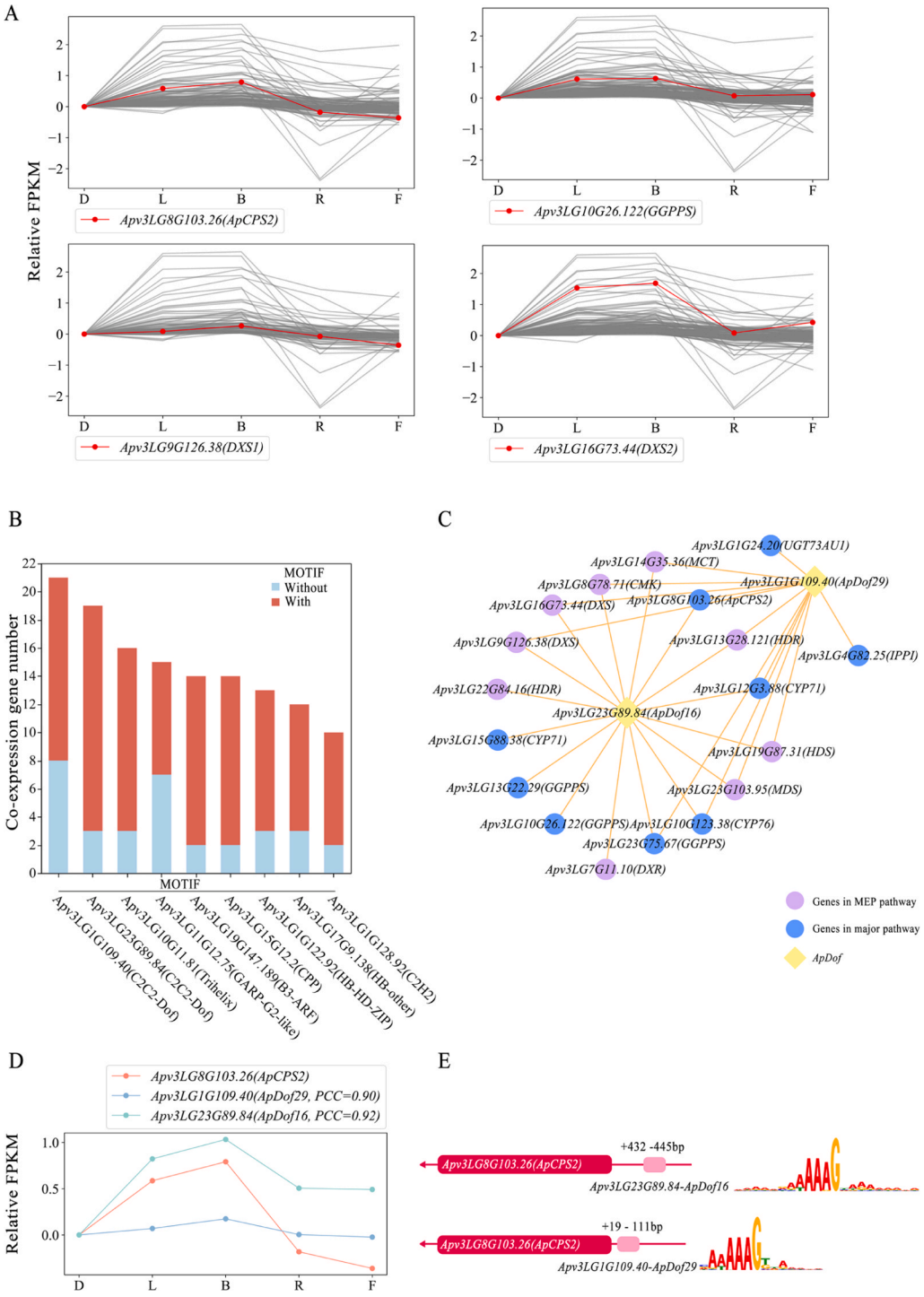

Fig. 3. Dof transcription factors potentially were involved in andrographolide biosynthesis. (A) Co-expression analysis was used to identify the TFs that were co-expressed with andrographolide biosynthesis related genes (ABRGs). Red lines indicated the ABRGs, while gray lines represent co-expressed TF. D: dark; L: white light; B: blue light; R: red light; F: far-red light. The relative FPKM indicated the $\log_{10}$ fold change relative to the average FPKM of the dark group (Group D). The identification of co-expressed TFs was conducted through the utilization of a PCC value greater than 0.7 and a p-value less than 0.05. (B) The number of the co-expressed ABRGs harbored with or without the corresponding TF motifs in their promoters. (C) Potential regulatory network of two Dof type transcription factors (*Apv3LG23G89.84* and *Apv3LG1G109.40*) and its potentially targeted ABRGs. Genes that have been annotated in purple are associated with the MEP pathway, while those in blue are linked to the major pathway. The genes that are indicated in yellow are two Dof type transcription factors. (D) The relative expression levels of *ApCPS2*, *ApDof29*, and *ApDof16* under various light treatments are presented. **(E)** Conserved DOF-binding motifs have been identified in the promoters of a key ABRGs, *ApCPS2*. The TFs Motif were identified as *Apv3LG23G89.84* (*ApDof16*) and *Apv3LG1G109.40* (*ApDof29*).

A. paniculata seedlings (Fig. 2B).

Together, these results supported that light could promote the andrographolide biosynthesis via modulating the intrinsic gene expression, especially the ABRGs.

3.2. Co-expression and motif analysis identified the Dof TF as key regulatory genes

As the transcription factors (TFs) play an important role in regulatory andrographolide (Guan et al., 2022; Kumar et al., 2024; Zhang et al., 2021a), to identify potential key TFs involved in light response, we first calculated the Pearson Correlation Coefficient (PCC) between the differentially expressed ABRGs and TFs. Gene pairs with a PCC of ≥ 0.7 and a p-value of ≤ 0.05 were considered as co-expressed gene pairs. A total of 1260 TFs co-expressed with ABRGs were found (Table S3). For example, two C2C2-Dofs, *Apv3LG23G89.84* (*ApDof16*) and, *Apv3LG1G109.40* (*ApDof29*) as well as *Apv3LG10G11.81* (*Trihelix*) TFs co-expressed with the *ApCPS2*, *GGPPS*, *DXS1* and *DXS2* were identified (Fig. 3A and Tables S3).

Furthermore, Motif scanning via FIMO software was then performed using the promoter sequences of the differentially expressed ABRGs and public TF motif databases to identify potential TF binding sites (Table S4). As the results showed, 772 TF binding motifs have been found in these co-expressed ABRGs and *ApDof16*, *ApDof29*, and *Trihelix*, were the top 10 TF motifs identified, suggesting their important roles in regulating the expression of ABRGs (Fig. 3B).

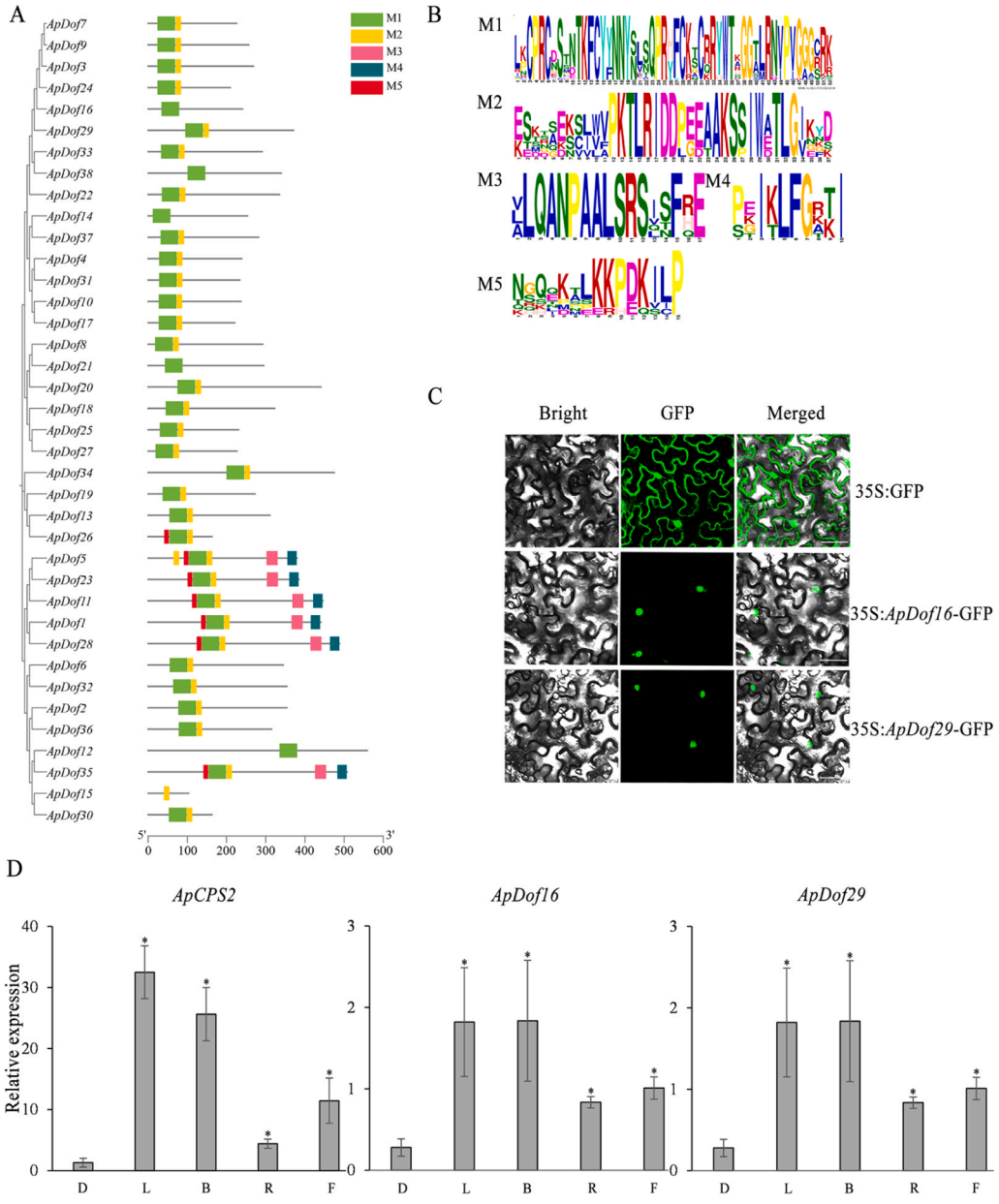

Fig. 4. Genomic charactization of the *ApDof16* and *ApDof29*. (A) Phylogenetic tree and motif analysis the Dof TF family in *A. paniculata.* The M1–5 indicated the five conversed protein motifs in this family. (B) The Position Weight Matrix of the five conversed protein motifs (M1-M5) in the Dof TF family. (C) The subcellular localization of *ApDof16* and *ApDof29*. Confocal microscopy images of tobacco epidermal cells expressing: 35S:GFP (empty vector control), 35S:*Dof16*-GFP and 35S:*Dof29*-GFP fusion proteins. Merged: GFP fluorescence (green channel) was overlaid on bright-field images. Scale bars = 50 μm. (D) The relative expression levels of *ApCPS2*, *ApDof29*, and *ApDof16* in different light treatments. L, B, R, F, and D represent *A. paniculata* seedlings grown under white light, blue light, red light, far-red light, and dark conditions, respectively. Expression levels were then normalized relative to the *Actin* gene. Data are presented as mean ± SE of three biological replicates. Asterisks (*) indicate the significant differences compared to the D group (p-value < 0.05, by Student's test).

As Fig. 3C shown, two co-expressed Dof genes, *ApDof16* and *ApDof29*, that have been found to potentially target many ABRGs (Table S5) such as the *ApCPS2*, *GGPPS* and *DXS* etc., especially in the MEP pathway. Among the 18 biosynthetic genes co-expressed with *ApDof16* and *ApDof29*, 9 belong to the MEP pathway, indicating a strong correlation between Dof transcription factors and MEP-related genes. As shown in Fig. 3D, the expression patterns of *ApDof16* and *ApDof29* are highly correlated with that of *ApCPS2* under different light treatments, with Pearson correlation coefficients (PCCs) of 0.92 and 0.90, respectively. Notably, both *ApDof16* and *ApDof29* show high expression levels under white (L) and blue (B), mirroring the increased expression of *ApCPS2*, a key gene in andrographolide biosynthesis. This strong co-expression pattern substantiates that *ApDof16* and *ApDof29* regulate *ApCPS2* and other MEP pathway genes in response to light, thereby modulating andrographolide biosynthesis. As shown in Fig. 3E, both *ApDof16* and *ApDof29* have predicted binding sites in the promoter region of *ApCPS2*, which further supported their regulatory roles. Sequence analysis of the *ApDof16* and *ApDof29* found that they harboured a conserved amino acid domain (M1), which is present in all Dofs. However, they do not share any other domains with other ApDof TFs in *A. paniculata* genome (Fig. 4A and Fig. 4B). In addition, gene structure analysis revealed that the majority of ApDof genes, including *ApDof16* and *ApDof29*, possess relatively simple, straightforward exon-intron structures, further corroborating their conservation (Table S6 and Figure S2). However, as the results of phylogenetic tree analysis, *ApDof16* and *ApDof29* belong to different clusters, suggesting that they may have divergent functions in the regulation of andrographolide (Figure S3).

As previously reported (Liu et al., 2018), Dof TF located in the nucleus to regulate gene expression, to confirm the subcellular localization of *ApDof16* and *ApDof29*, we constructed the 35S:*ApDof16*-GFP and 35S:*ApDof29*-GFP vectors and transiently transformed them into tobacco leaves. In contrast to the empty control (35S: GFP), ApDof16 and ApDof29 proteins were observed the localization in the nucleus, suggesting their transcriptional activity in this compartment (Fig. 4C). Additionally, qPCR analysis showed that the expression levels of *ApCPS2*, *ApDof16*, and *ApDof29* were significantly induced by light treatments, especially under white and blue light conditions, compared to the dark-grown seedlings (Fig. 4D), which is consistent with Fig. 1A.

3.3. Functional validation of the ApDof16 and ApDof29

As there is currently a lack of transgenic or genome-editing systems for *A. paniculata*, the virus-induced gene silencing (VIGS) method was employed for functional validation of these two Dof TFs. We constructed two VIGS vectors for *ApDof16* and *ApDof29* (see Method), and then transiently transformed them into *A. paniculata* via the Agrobacterium-mediated method. As results showed (Fig. 5), andrographolide content decreased significantly in the silencing lines of both *ApDof16* and *ApDof29* compared to the empty vector control. Gene expression analysis revealed that in *ApDof29* silencing lines, the expression of the key biosynthetic gene *ApCPS2* was significantly downregulated. However, no significant change in *ApCPS2* expression was observed in the *ApDof16* silencing lines (Fig. 5A and Fig. 5B). These data suggested that *ApDof29* could regulate andrographolide content via regulating *ApCPS2* expression. In contrast, the regulatory role of *ApDof16* is more complex. Although it is essential for andrographolide accumulation, its mechanism appears to be independent of *ApCPS2* transcriptional activation.

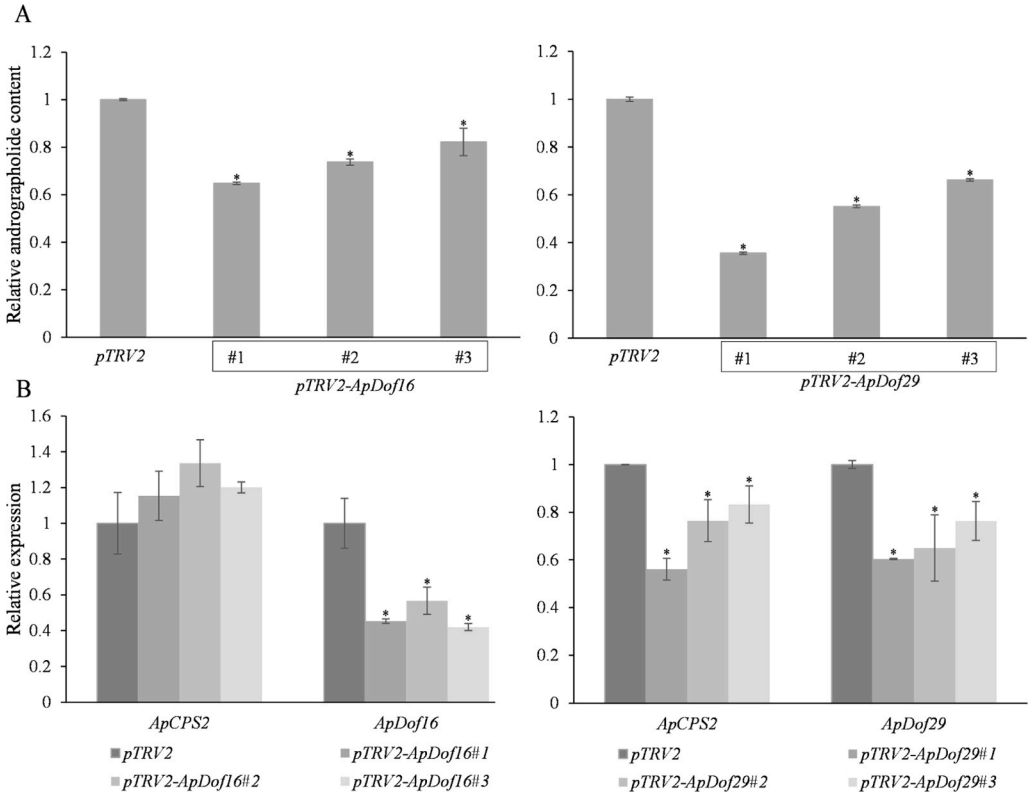

Fig. 5. Functional validation of *ApDof16* and *ApDof29* in the regulation of andrographolide biosynthesis. (A) Virus-induced gene silencing (VIGS) of *ApDof29* and *ApDof16* significantly reduced andrographolide accumulation. Relative andrographolide content in the control plants (pTRV2, empty vector) and VIGS lines was normalized to the average of the control group. Data are presented as mean ± SE (n = 3 biological replicates). Asterisks (*) indicate statistically significant differences compared to the control group (*p*-value < 0.05, by Student's *t*-test). **(B)** Real-time qPCR analysis of relative expression levels for *ApCPS2*, *ApDof29*, and *ApDof16* in control plants (infiltrated with the empty vector pTRV2) and three independent VIGS lines for *ApDof29* (#1, #2, #3) and *ApDof16* (#1, #2, #3). Asterisks (*) denote statistically significant differences compared to the control group (*p*-value < 0.05, by Student's *t*-test).

3.4. *ApDof29* but not *ApDof16* directly binds to the *ApCPS2* promoter

Given that both *ApDof16* and *ApDof29* are essential for andrographolide accumulation but show differential effects on *ApCPS2* transcription, we next sought to determine whether they directly bind to the *ApCPS2* promoter (*pApCPS2*). Firstly, in a Yeast One-Hybrid (Y1H) experiment, the *pApCPS2* sequence was cloned into the pAbAi vector, while the *ApDof16* and *ApDof29* were then separately cloned into the pGADT7 vector. Interestingly, as shown in Fig. 6A, yeast expressing ApDof29 grew robustly on the selective medium containing Aureobasidin A (SD/-Leu+AbA300), indicating a direct binding interaction. Conversely, no growth was observed for yeast expressing ApDof16 or the empty vector control. The Y1H assay revealed that only ApDof29, rather than ApDof16 that could directly bind to ApCPS2. To further confirm this observation, we performed a transient assay. The *pApCPS2* was cloned into the upstream of the luciferase (LUC) genes as the reporter, while the *ApDof16* and *ApDof29* were cloned into the downstream of the 35S promoter, serving as effectors. As shown in Fig. 6B, a strong luminescence signal was observed when the *pApCPS2*:LUC reporter was co-expressed with 35S:*ApDof29*, whereas co-expression with 35S:*ApDof16* resulted in a LUC activity with no significant change compared to the empty vector control. As with the Y1H assay, 35S:*ApDof29* but not 35S:*ApDof16* was able to upregulate the *pApCPS2*:LUC reporter. Chromatin immunoprecipitation followed by qPCR analysis (ChIP-qPCR) was also used for analysis of the interaction between the Dofs and the *ApCPS2*. We transiently expressed the 35S:*ApDof29*-GFP and 35S:*ApDof16*-GFP in the leaves of *A. paniculata* and performed the ChIP-qPCR assay. After chromatin immunoprecipitation by the Anti-GFP antibody and DNA recovery, several real-time primers (P1 to P7) around the TSS of *ApCPS2* were designed (Fig. 6C). Among them, P5 and P6 primers were close to the Dof binding motifs. Compared to the input control, significant enrichment was observed in the ChIP assay of 35S:*ApDof29*-GFP in the P4, P5 and P6 regions of *pApCPS2*.However, such enrichment at the *pApCPS2* was not detected in the ChIP assay of 35S:*ApDof16*-GFP (Fig. 6D).

Together, these findings indicate that *ApDof29* can directly bind to *ApCPS2* to regulate andrographolide biosynthesis. In contrast, it remains unclear whether *ApDof16* regulates andrographolide production by targeting other ABRGs. Given the co-expression results, *ApDof16* is potentially associated with several genes in the MEP pathway, which may contribute to the observed reduction in andrographolide content following *ApDof16* silencing via VIGS. Nevertheless, further experimental validation is required to determine whether *ApDof16* directly regulates these MEP-related genes and to clarify its role in andrographolide biosynthesis.

4. Discussion

Andrographolide is one of the valuable bioactive medicinal compounds that is specifically accumulated in *A. paniculata*, a traditional Chinese medicinal plant (Chao and Lin, 2010; Vetvicka and Vannucci, 2021b). In our primary data and in previous reports (Srinath et al., 2022b; Sun et al., 2019b), Andrographolide is influenced by light, but the underlying mechanism is still unknown. In this study, we performed

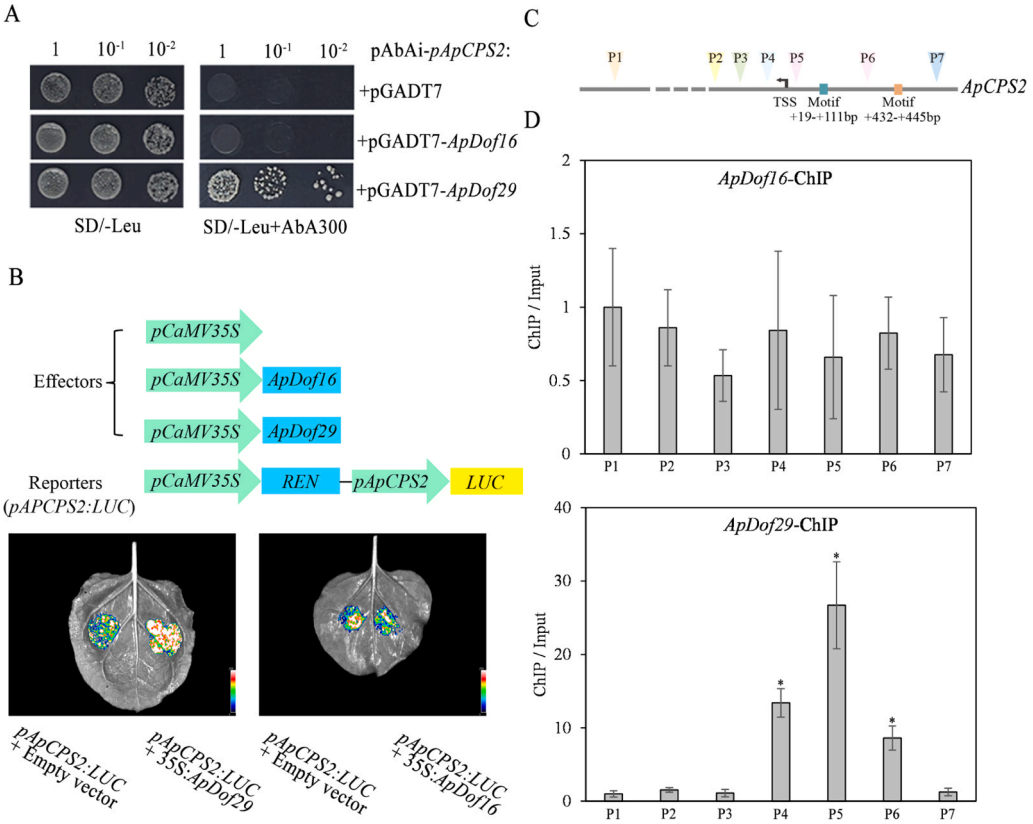

Fig. 6. *ApDof29* rather than *ApDof16* directly binds to the *ApCPS2* promoter. (A) Yeast one-hybrid (Y1H) assay demonstrating the binding of *ApDof16* and *ApDof29* to the *ApCPS2* promoter (*pApCPS2*). Transformants were selected on SD/-Leu medium supplemented with 300 ng/mL aureobasidin A (AbA). Experimental groups: pAbAi-*pApCPS2* + pGADT7-*ApDof16* and pAbAi-*pApCPS2* + pGADT7-*ApDof29*; control group: pAbAi-*pApCPS2* + pGADT7. The vector pGADT7 is the empty vector. **(B)** Transient dual-luciferase reporter assay to evaluate the regulatory effects of *ApDof16* and *ApDof29* on the *pApCPS2*. Upper panel: The vector construction of the effectors and the reporters. Lower panel: The luciferase activity from co-infiltration of the *pApCPS2*:LUC reporter and effector plasmids carrying the empty vector (pGreenII 62-SK), 35S: *ApDof16*, or 35S: *ApDof29*. **(C)** Primer design surrounding the transcriptional start site (TSS) of *pApCPS2* for the ChIP-qPCR assay. **(D)** ChIP-qPCR analysis of enrichment signals using 35S: *ApDof16*-GFP and 35S: *ApDof29*-GFP constructs. The relative enrichment signal is represented by the ChIPed DNA versus the input DNA. Asterisks (*) indicate significant differences compared to the P1 region (p-value < 0.05, by Student's t-test).

bioinformatics analysis using the RNA-seq data from various light treatments and identified a key light-induced TF, *ApDof29,* that promotes the andrographolide biosynthesis by directly binding to the *ApCPS2*.

Indeed, there are two Dof TFs that can regulate the andrographolide biosynthesis were found in the VIGS experiments. Silencing of the *ApDof16* or *ApDof29* downregulates the andrographolide content as well as the *ApCPS2* expression. However, with the molecular evidence from Y1H, transient assays and the ChIP-qPCR experiment, *ApDof16* was clearly to shown no direct binding activity on *ApCPS2* promoter. Additionally, unlike *ApDof29*, *ApDof16* does not exhibit similar expression patterns to *ApCPS2* in various tissues (Figure S4). This apparent discrepancy suggests that *ApDof16* may not act as a direct activator of the *ApCPS2* but instead exerts its positive regulatory effect through a more complex manner (e.g. via epigenetic factors) (Gupta et al., 2015; Huang et al., 2024; Ruta et al., 2020). One possibility is that it regulates the expression of other ABRGs in the biosynthesis pathway, which need further investigation.

Nevertheless, given the vital functional role of ApDofs in regulating the secondary metabolites (e.g. andrographolide), these two TFs might serve as the key candidates for the further molecular breeding of *A. paniculata*. In addition, as the cost of DNA resequencing continues to decline, identifying haplotype variations in Dof (transcription factors) through large-scale data analysis has emerged as another rapid molecular breeding strategy for *A. paniculata* (Wu et al., 2019; Xia et al., 2020). Another molecular breeding approach in *A. paniculata* is the establishment of transgenic systems for the overexpress of these Dof TFs driven by specific regulatory elements (Lv et al., 2025; Tang et al., 2014; Zhang et al., 2016).

As shown in Fig. 1A, andrographolide is upregulated by light. However, different qualities of light have distinct effects on the andrographolide biosynthesis. Furthermore, blue light is optimal for the andrographolide biosynthesis compared to Red and Far-red light. The precise control of light quality and duration offered by LED technology plays a pivotal role in triggering the biosynthesis pathways of secondary metabolites in medicinal plants (Ahmadi et al., 2021; Livadariu et al., 2023; Sabzalian et al., 2014). These findings suggest that blue light could be integrated into a smart greenhouse cultivation system for andrographolide production. However, the LED lighting conditions would need to be optimized further for this system.

5. Conclusion

Overall, our study reveals the regulatory role of Dof transcription factors in light-induced andrographolide biosynthesis in *A. paniculata*. In particular, the up-regulated Dof, *ApDof29*, may be important biotechnological resource for increasing andrographolide content.

CRediT authorship contribution statement

Yanqin Xu: Writing – review & editing. **Ling Zhang:** Supervision, Funding acquisition, Conceptualization. **Xingbin Lv:** Writing – original draft, Visualization, Software, Data curation. **Zhiyi Zhang:** Writing – review & editing. **Mingkun Huang:** Writing – review & editing. **Tingting Jing:** Validation. **Ying Xiong:** Validation. **Hua Yang:** Writing – original draft, Validation. **Yufang Hu:** Validation. **Qi Liang:** Software, Data curation. **Shuyun Tian:** Visualization, Software. **Lang Yang:** Validation.

Declaration of Competing Interest

The authors declare that they have no known competing financial interests or personal relationships that could have appeared to influence the work reported in this paper.

Acknowledgements

This work was supported by the National Natural Science Foundation of China (82260745) and Jiangxi Provincial Natural Science Foundation (20232BAB216120, China).

Appendix A. Supporting information

Supplementary data associated with this article can be found in the online version at doi:10.1016/j.indcrop.2025.121715.

Data availability

Data will be made available on request.

References

Ahmadi, T., Shabani, L., Sabzalian, M.R., 2021. LED light sources improved the essential oil components and antioxidant activity of two genotypes of lemon balm (Melissa officinalis L.). Bot. Stud. 62, 9. https://doi.org/10.1186/s40529-021-00316-7.

Armarego-Marriott, T., Sandoval-Ibañez, O., Kowalewska, Ł., 2020. Beyond the darkness: recent lessons from etiolation and de-etiolation studies. J. Exp. Bot. 71, 1215–1225. https://doi.org/10.1093/jxb/erz496.

Cao, Q., Dong, P., Han, H., 2024. Therapeutic effects of the major alkaloid constituents of evodia rutaecarpa in Alzheimer's disease. Psychogeriatr. Off. J. Jpn. Psychogeriatr. Soc. 24, 443–457. https://doi.org/10.1111/psyg.13051.

Chalichem, N.S.S., Nabhan, P., Bethapudi, B., Agarwal, N., Murugan, S.K., Deepak, M., 2024. Assessment of immunomodulatory activity of AP-Bio® (KalmCold®), a standardized extract of andrographis paniculata using in vivo and ex vivo models. Pharmacogn. Mag. https://doi.org/10.1177/09731296231222378.

Chao, W.-W., Lin, B.-F., 2010. Isolation and identification of bioactive compounds in andrographis paniculata (Chuanxinlian). Chin. Med. 5, 17. https://doi.org/10.1186/1749-8546-5-17.

Chen, C., Wu, Y., Li, J., Wang, X., Zeng, Z., Xu, J., Liu, Y., Feng, J., Chen, H., He, Y., Xia, R., 2023a. TBtools-II: a "one for all, all for one" bioinformatics platform for biological big-data mining. Mol. Plant 16, 1733–1742. https://doi.org/10.1016/j.molp.2023.09.010.

Chen, L.-M., Gao, H.-M., Zhu, J.-J., Feng, W.-H., Liu, X.-Q., Yan, L.-H., Zhang, Y.-X., Meng, C.-X.-N., Wang, Z.-M., Wang, D.-Q., 2020. Effects of different harvesting and processing methods on quality of andrographis herba. Zhongguo Zhong Yao Za Zhi Zhongguo Zhongyao Zazhi China J. Chin. Mater. Med. 45, 1717–1725. https://doi.org/10.19540/j.cnki.cjcmm.20200106.201.

Chen, X., Ren, J., Yang, J., Zhu, Z., Chen, R., Zhang, L., Chen, X., Ren, J., Yang, J., Zhu, Z., Chen, R., Zhang, L., 2023b. A critical review of *andrographis paniculata*. Med. Plant Biol. 2. https://doi.org/10.48130/MPB-2023-0015.

Cn, C., Ty, L., Yc, H., Gz, L., Kc, T., Yh, L., Pl, K., Hq, Z., Wc, C., 2019. PlantPAN3.0: a new and updated resource for reconstructing transcriptional regulatory networks from ChIP-seq experiments in plants. Nucleic Acids Res 47. https://doi.org/10.1093/nar/gky1081.

Gao, S., Xu, T., Wang, W., Li, J., Shan, Y., Wang, Y., Tan, H., 2025b. Polysaccharides from anemarrhena asphodeloides bge, the extraction, purification, structure characterization, biological activities and application of a traditional herbal Medicine. Int. J. Biol. Macromol. 311, 143497. https://doi.org/10.1016/j.ijbiomac.2025.143497.

Gao, S., Wang, Y., Shan, Y., Wang, W., Li, J., Tan, H., 2025a. Rhizoma coptidis polysaccharides: extraction, separation, purification, structural characteristics and bioactivities. Int. J. Biol. Macromol. 320, 145677. https://doi.org/10.1016/j.ijbiomac.2025.145677.

Gonde, D.P., Bhole, B.K., Kakad, K.S., 2024. Andrographolide, diterpenoid constituent of *andrographis paniculata*: review on botany, phytochemistry, molecular docking analysis, and pharmacology. Ann. Pharm. Fr. 82, 15–43. https://doi.org/10.1016/j.pharma.2023.10.001.

Grant, C.E., Bailey, T.L., Noble, W.S., 2011. FIMO: scanning for occurrences of a given motif. Bioinformatics 27, 1017. https://doi.org/10.1093/bioinformatics/btr064.

Guan, R., Xu, S., Lu, Z., Su, L., Zhang, L., Sun, W., Zhang, Y., Jiang, C., Liu, Z., Duan, L., Ji, A., 2022. Genomic characterization of bZIP transcription factors related to andrographolide biosynthesis in andrographis paniculata. Int. J. Biol. Macromol. 223, 1619–1631. https://doi.org/10.1016/j.ijbiomac.2022.10.283.

Gupta, S., Malviya, N., Kushwaha, H., Nasim, J., Bisht, N.C., Singh, V.K., Yadav, D., 2015. Insights into structural and functional diversity of dof (DNA binding with one finger) transcription factor. Planta 241, 549–562. https://doi.org/10.1007/s00425-014-2239-3.

Huang, M., Hu, Y., Zhang, L., Yang, H., Feng, C., Jiang, C., Xie, N., Liu, D., Chen, S., Wang, J., Sun, W., 2024. Decoding the chromatin accessibility in *andrographis paniculata* genome, a case study of genome-wide investigation of the *cis*-regulatory elements in medicinal plants. Acta Pharm. Sin. B 14, 4179–4182. https://doi.org/10.1016/j.apsb.2024.06.012.

Intharuksa, A., Arunotayanun, W., Yooin, W., Sirisa-ard, P., 2022. A comprehensive review of andrographis paniculata (Burm. f.) nees and its constituents as potential lead compounds for COVID-19 drug discovery. Molecules 27, 4479. https://doi.org/10.3390/molecules27144479.

Jiang, Z., Xu, G., Jing, Y., Tang, W., Lin, R., 2016. Phytochrome b and REVEILLE1/2-mediated signalling controls seed dormancy and germination in arabidopsis. Nat. Commun. 7, 12377. https://doi.org/10.1038/ncomms12377.
Jones, M.A., 2018. Using light to improve commercial value. Hortic. Res. 5, 1–13. https://doi.org/10.1038/s41438-018-0049-7.
K, S., Pk, S., G, K., 2006. Antioxidant and anti-inflammatory activities of the plant andrographis paniculata nees. Immunopharmacol. Immunotoxicol. 28. https://doi.org/10.1080/08923970600626007.
Kim, D., Paggi, J.M., Park, C., Bennett, C., Salzberg, S.L., 2019. Graph-based genome alignment and genotyping with HISAT2 and HISAT-genotype. Nat. Biotechnol. 37, 907–915. https://doi.org/10.1038/s41587-019-0201-4.
Kumar, R., Kumar, Chavlesh, Roy Choudhury, D., Ranjan, A., Raipuria, R.K., Dubey, K.K. D., Mishra, A., Kumar, Chetan, Manzoor, M.M., Kumar, A., Kumari, A., Singh, K., Singh, G.P., Singh, R., 2024. Isolation, characterization, and expression analysis of NAC transcription factor from andrographis paniculata (Burm. f.) nees and their role in andrographolide production. Genes 15, 422. https://doi.org/10.3390/genes15040422.
Kusnetsov, V.V., Doroshenko, A.S., Kudryakova, N.V., Danilova, M.N., 2020. Role of phytohormones and light in De-etiolation. Russ. J. Plant Physiol. 67, 971–984. https://doi.org/10.1134/S1021443720060102.
Lee, H.-J., Park, Y.-J., Ha, J.-H., Baldwin, I.T., Park, C.-M., 2017. Multiple routes of light signaling during root photomorphogenesis. Trends Plant Sci. 22, 803–812. https://doi.org/10.1016/j.tplants.2017.06.009.
Li, X., Yuan, W., Wu, J., Zhen, J., Sun, Q., Yu, M., 2022. Andrographolide, a natural anti-inflammatory agent: an update. Front. Pharm. 13. https://doi.org/10.3389/fphar.2022.920435.
Liu, Y., Li, P., Fan, L., Wu, M., 2018. The nuclear transportation routes of membrane-bound transcription factors. Cell Commun. Signal 16, 12. https://doi.org/10.1186/s12964-018-0224-3.
Livadariu, O., Maximilian, C., Rahmanifar, B., Cornea, C.P., 2023. LED technology applied to plant development for promoting the accumulation of bioactive compounds: a review. Plants 12, 1075. https://doi.org/10.3390/plants12051075.
Lv, X., Yang, H., Hu, Y., Liang, Q., Tian, S., Yang, L., Huang, M., Zhang, L., Xu, Y., 2025. Genomic characterization and functional validation of six cis-Regulatory sequences in medicinal plant andrographis paniculata. Horticulturae 11, 63. https://doi.org/10.3390/horticulturae11010063.
Okhuarobo, A., Falodun, J.E., Erharuyi, O., Imieje, V., Falodun, A., Langer, P., 2014. Harnessing the medicinal properties of andrographis paniculata for diseases and beyond: a review of its phytochemistry and pharmacology. Asian Pac. J. Trop. Dis. 4, 213. https://doi.org/10.1016/S2222-1808(14)60509-0.
Paul, S., Roy, D., Pati, S., Sa, G., 2021. The adroitness of andrographolide as a natural weapon against colorectal cancer. Front. Pharm. 12. https://doi.org/10.3389/fphar.2021.731492.
Pereira, J., Mouazen, A.M., Foo, M., Ahmed, H., 2021. A framework of artificial light management for optimal plant development for smart greenhouse application. PLOS ONE 16, e0261281. https://doi.org/10.1371/journal.pone.0261281.
Ruta, V., Longo, C., Lepri, A., De Angelis, V., Occhigrossi, S., Costantino, P., Vittorioso, P., 2020. The DOF transcription factors in seed and seedling development. Plants 9, 218. https://doi.org/10.3390/plants9020218.
Sabzalian, M.R., Heydarizadeh, P., Zahedi, M., Boroomand, A., Agharokh, M., Sahba, M. R., Schoefs, B., 2014. High performance of vegetables, flowers, and medicinal plants in a red-blue LED incubator for indoor plant production. Agron. Sustain. Dev. 34, 879–886. https://doi.org/10.1007/s13593-014-0209-6.
Smitha, G.R., Gajbhiye, N.A., Tripathy, V., 2020. Influence of drying methods and packaging materials on physico-chemical properties and phytochemical composition of *kalmegh* [*andrographis paniculata* (Burm. f.) Wall. ex Nees] for shelf life enhancement. Med. Plants Int. J. Phytomedicines Relat. Ind. 12, 227. https://doi.org/10.5958/0975-6892.2020.00030.1.
Srinath, M., Shailaja, A., Bindu, B.B.V., Giri, C.C., 2022a. Comparative analysis of biomass, ethrel elicitation, light induced differential MVA/MEP pathway gene expression and andrographolide production in adventitious root cultures of andrographis paniculata (Burm. F.) nees. Plant Cell Tissue Organ Cult. PCTOC 149, 335–349. https://doi.org/10.1007/s11240-022-02241-4.
Srinath, M., Shailaja, A., Bindu, B.B.V., Giri, C.C., 2022b. Comparative analysis of biomass, ethrel elicitation, light induced differential MVA/MEP pathway gene expression and andrographolide production in adventitious root cultures of andrographis paniculata (Burm. F.) nees. Plant Cell Tissue Organ Cult. PCTOC 149, 335–349. https://doi.org/10.1007/s11240-022-02241-4.
Sun, W., Leng, L., Yin, Q., Xu, M., Huang, M., Xu, Z., Zhang, Y., Yao, H., Wang, C., Xiong, C., Chen, Sha, Jiang, C., Xie, N., Zheng, X., Wang, Y., Song, C., Peters, R.J., Chen, Shilin, 2019b. The genome of the medicinal plant andrographis paniculata provides insight into the biosynthesis of the bioactive diterpenoid neoandrographolide. Plant J. 97, 841–857. https://doi.org/10.1111/tpj.14162.
Sun, W., Leng, L., Yin, Q., Xu, M., Huang, M., Xu, Z., Zhang, Y., Yao, H., Wang, C., Xiong, C., Chen, Sha, Jiang, C., Xie, N., Zheng, X., Wang, Y., Song, C., Peters, R.J., Chen, Shilin, 2019a. The genome of the medicinal plant andrographis paniculata provides insight into the biosynthesis of the bioactive diterpenoid neoandrographolide. Plant J. 97, 841–857. https://doi.org/10.1111/tpj.14162.
Tamura, K., Stecher, G., Kumar, S., 2021. MEGA11: molecular evolutionary genetics analysis version 11. Mol. Biol. Evol. 38, 3022–3027. https://doi.org/10.1093/molbev/msab120.
Tang, K., Shen, Q., Yan, T., Fu, X., 2014. Transgenic approach to increase artemisinin content in artemisia annua l. Plant Cell Rep. 33, 605–615. https://doi.org/10.1007/s00299-014-1566-y.
Uttekar, M.M., Das, T., Pawar, R.S., Bhandari, B., Menon, V., Nutan, Gupta, S.K., Bhat, S. V., 2012. Anti-HIV activity of semisynthetic derivatives of andrographolide and computational study of HIV-1 gp120 protein binding. Eur. J. Med. Chem. 56, 368–374. https://doi.org/10.1016/j.ejmech.2012.07.030.
Vetvicka, V., Vannucci, L., 2021b. Biological properties of andrographolide, an active ingredient of andrographis paniculata: a narrative review. Ann. Transl. Med. 9, 1186. https://doi.org/10.21037/atm-20-7830.
Vetvicka, V., Vannucci, L., 2021a. Biological properties of andrographolide, an active ingredient of andrographis paniculata: a narrative review. Ann. Transl. Med. 9, 1186. https://doi.org/10.21037/atm-20-7830.
Wu, D., Liang, Z., Yan, T., Xu, Y., Xuan, L., Tang, J., Zhou, G., Lohwasser, U., Hua, S., Wang, H., Chen, X., Wang, Q., Zhu, L., Maodzeka, A., Hussain, N., Li, Z., Li, X., Shamsi, I.H., Jilani, G., Wu, L., Zheng, H., Zhang, G., Chalhoub, B., Shen, L., Yu, H., Jiang, L., 2019. Whole-Genome resequencing of a worldwide collection of rapeseed accessions reveals the genetic basis of ecotype divergence. Mol. Plant 12, 30–43. https://doi.org/10.1016/j.molp.2018.11.007.
Xia, E., Tong, W., Hou, Y., An, Y., Chen, L., Wu, Q., Liu, Y., Yu, J., Li, F., Li, R., Li, P., Zhao, H., Ge, R., Huang, J., Mallano, A.I., Zhang, Y., Liu, S., Deng, W., Song, C., Zhang, Zhaoliang, Zhao, J., Wei, S., Zhang, Zhengzhu, Xia, T., Wei, C., Wan, X., 2020. The reference genome of tea plant and resequencing of 81 diverse accessions provide insights into its genome evolution and adaptation. Mol. Plant 13, 1013–1026. https://doi.org/10.1016/j.molp.2020.04.010.
Zhang, L., Yung, W.-S., Hu, Y., Wang, L., Sun, W., Huang, M., Zhang, L., Yung, W.-S., Hu, Y., Wang, L., Sun, W., Huang, M., 2023. Establishment of a convenient ChIP-seq protocol for identification of the histone modification regions in the medicinal plant *andrographis paniculata*. Med. Plant Biol. 2. https://doi.org/10.48130/MPB-2023-0006.
Zhang, R., Chen, Z., Liao, B., Duan, L., Ji, A., 2021a. Genomic characterization of WRKY transcription factors related to andrographolide biosynthesis in andrographis paniculata. Front. Genet 11. https://doi.org/10.3389/fgene.2020.601689.
Zhang, S., Zhang, L., Zou, H., Qiu, L., Zheng, Y., Yang, D., Wang, Y., 2021b. Effects of light on secondary metabolite biosynthesis in medicinal plants. Front. Plant Sci. 12. https://doi.org/10.3389/fpls.2021.781236.
Zhang, Y., Liang, Z., Zong, Y., Wang, Y., Liu, J., Chen, K., Qiu, J.-L., Gao, C., 2016. Efficient and transgene-free genome editing in wheat through transient expression of CRISPR/Cas9 DNA or RNA. Nat. Commun. 7, 12617. https://doi.org/10.1038/ncomms12617.
Zheng, Y., Jiao, C., Sun, H., Rosli, H.G., Pombo, M.A., Zhang, P., Banf, M., Dai, X., Martin, G.B., Giovannoni, J.J., Zhao, P.X., Rhee, S.Y., Fei, Z., 2016. iTAK: a program for Genome-wide prediction and classification of plant transcription factors, transcriptional regulators, and protein kinases. Mol. Plant 9, 1667–1670. https://doi.org/10.1016/j.molp.2016.09.014.